Decision Support in Peripheral Arterial Occlusive Disease Management with AI-Enhanced Super-Resolution Techniques for Advanced Vascular Imaging

Alexandra La Cruz[0000−0001−6052−2933],
Juan Pedro Felipe,
Erika Severeyn[0000−0002−9500−3532], and
Andrés García-León[0000−0003−1757−6885]

Abstract Peripheral Arterial Occlusive Disease (PAOD) management is essential in combating atherosclerosis-induced blockages, requiring advanced vascular imaging for accurate diagnosis and treatment. Artificial intelligence-enhanced super-resolution (SR) techniques are increasingly recognized for improving vascular imaging and decision support, enhancing PAOD treatment accuracy and efficacy. PAOD, caused by atherosclerosis, reduces blood flow to the lower extremities. Computed tomography angiography (CTA) images are used for evaluating PAOD, offering detailed visualization of vascular structures. This study used CTA images, the most common modality for daily PAOD evaluation, to demonstrate the role of SR techniques in decision support systems, particularly in healthcare. The research addresses challenges in segmenting CTA images of lower extremity arteries, highlighting SR techniques' potential in refining artery segmentation, 3D modeling, and visualization. Comparing SR models like SRCNN, EDSR, RCAN, SRGAN, and ESRGAN, the study identifies SRGAN as the optimal choice. These are models based on deep learning and generative models. Metrics like peak signal-to-noise ratio (PSNR) and structural similarity (SSIM) validate model efficacy. This sophisticated technology aids healthcare professionals in making smarter decisions, analyzing complex information, and providing valuable recommendations.

Alexandra La Cruz
Faculty of Engineering, Universidad de Ibagué, Ibagué, Tolima, Colombia, e-mail: alexandra.lacruz@unibague.edu.co

Juan Pedro Felipe
Computer Engineer and Biomedical Engineering, Universidad Internacional de Valencia, Valencia, España, e-mail: Felipe@gmail.com

Erika Severeyn
Department of Thermodynamics and Transfer Phenomena, Universidad Simón Bolívar, Venezuela, e-mail: severeynerika@usb.ve

Andrés García-León
Tecnologico de Monterrey, Escuela de Ingeniería y Ciencias, e-mail: andres.garcialeon@tec.mx

1 Introduction

Different epidemiological studies have shown that up to 50% of patients with the PAOD [4] have symptoms of cerebrovascular or cardiological disease, a real cause of patient morbidity and mortality [24]. PAOD describes a narrowing (stenosis) or complete blockage (occlusion) of the arteries of the arm or leg (see Fig. 1) [4]. PAOD can cause leg pain when walking (intermittent claudication), which may go

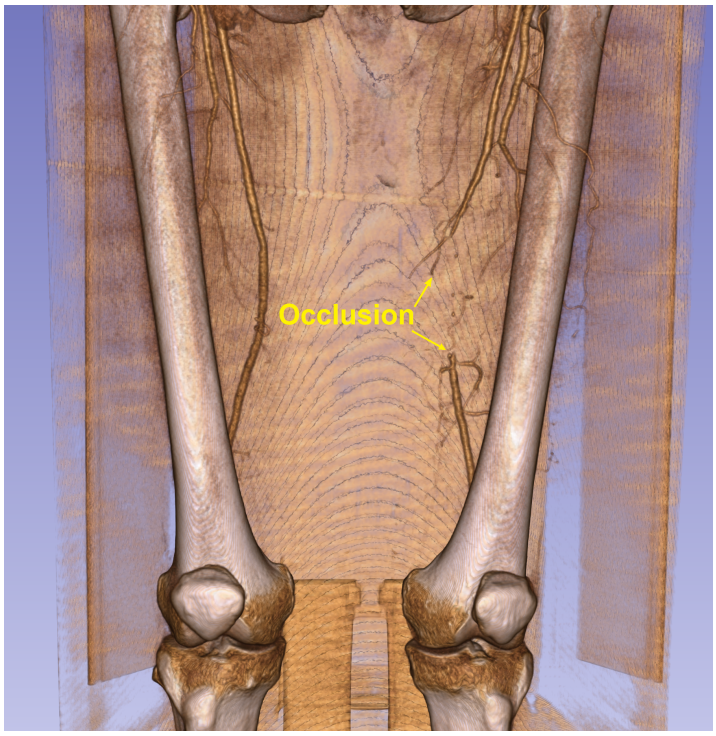

Fig. 1 3D visualization of a PAOD case of a patient. The arrows indicate the begin-ends of the occlusion.

away with rest. Over time, the disease can worsen and there may be pain even at rest, leg ulcers, and, in severe cases, gangrene, which may lead to amputation of the affected limb [4]. Consequently, in patients with PAOD, atherosclerotic stenosis is likely to appear in other areas of the body, such as in the coronary arteries and cerebral arteries. Mortality and morbidity caused by PAOD will depend largely on poor circulation in these areas rather than on limb ischemia [4, 1].

The best way to visualize vascular structures for patients with PAOD is through advanced imaging techniques such as computed tomography angiography (CTA), magnetic resonance angiography (MRA), or duplex ultrasoundD [22]. These imaging modalities provide detailed visualization of the vascular structures in the affected

limbs, allowing healthcare providers to assess the extent of arterial narrowing or blockages and plan appropriate treatment strategies. In this work, the study was made using CTA images, which are the most used image modality for daily and real-world evaluation of PAOD patients. On the other hand, in the context of PAOD, thee-dimensional (3D) reconstruction and visualization of vascular structures using CTA can provide a comprehensive view of the arteries, including the location and severity of stenosis or occlusionsg [26]. This 3D model can help clinicians in planning interventions such as angioplasty, stenting, or bypass surgery [38]. SR techniques have the ability to improve the quality of 3D models in regions with tiny blood vessels; conventional SR methods, such as interpolation, encounter limitations, especially with low-resolution images. Despite difficulties such as data acquisition and processing time, the integration of 3D rendering significantly improves the assessment and treatment of PAOD by providing accurate anatomical information and promoting collaborative decision making among healthcare professionals [21]. Moreover, beyond its utility in PAOD, 3D modeling and visualization play a crucial role in surgical planning, simulation, training, and augmented reality applications [33].

Conversely, the tiny diameter of some areas of blood vessels poses significant challenges for 3D rendering, requiring careful consideration of several factors. Ensuring high spatial resolution through techniques like computed tomography angiography (CTA) or magnetic resonance angiography (MRA) is vital for capturing intricate details accurately, as smaller vessels require more data points for precise 3D reconstruction. AAdditionally, the use of noise reduction methods, advanced vessel segmentation algorithms or super-resolution (SR) techniques is crucial to improve image resolution. Still, the visualization of small blood vessels, especially with atherosclerosis, is a challenge [18]. Healthy arteries show a uniform CT density due to contrast-enhanced blood, which has higher x-ray attenuation than soft tissues and lower than bone. Diseased arteries vary in x-ray attenuation: non-calcified plaque matches soft tissues, while calcified plaque resembles bone. Additionally, factors like image noise, scanning artifacts, limited resolution, and variability in arterial opacification must be considered. Despite these challenges, ongoing advancements in imaging technology and software promise continued improvements in 3D visualization capabilities. SR techniques, in particular, have the potential to enhance the quality and definition of 3D models, especially in regions with tiny blood vessels. Nevertheless, conventional SR techniques like interpolation methods have limitations, particularly with low-resolution images.

This chapter specifically delves into the effectiveness of various SR techniques based on deep learning and generative models, evaluating their impact on improving the diagnosis and well-being of patients suffering from PAOD by processing CTA images of the lower extremities. The application of these advanced SR techniques in CTA imaging is ready to improve diagnostic accuracy and treatment planning, which will ultimately benefit patients. By enhancing the accuracy of 3D visualization, these techniques aim to provide clinicians with more robust decision support tools. The chosen models encompass a range of SR techniques, including the Super-Resolution using Convolutional Neural Network (SRCNN 915

and SRCNN 955 [7]), Enhanced Deep Residual Networks for Single Image Super Resolution (EDSR)[20], Residual Channel Attention Networks (RCAN)[36], Super-Resolution using Generative Adversarial Network (SRGAN)[29], and Enhanced Super-Resolution Generative Adversarial Networks (ESRGAN)[34]. The studied methods, typically used for processing natural color images, have been adapted for CTA image processing. In essence, this chapter underscores how technology is evolving to assist us in making smarter choices. By addressing the challenges in visualizing small blood vessels, particularly in patients with atherosclerotic disease, and leveraging advanced imaging techniques and SR methods, we highlight the potential for significant improvements in medical diagnostics and decision support, ultimately enhancing patient care.

The paper follows a structured approach with five key sections: (1) Section 2 provides a literature review and research context, (2) Section 3 details the methodology encompassing dataset and SR techniques, (3) Section 4 presents our findings, (4) Section 5 engages in an in-depth discussion of results and their relevance to existing knowledge, and concludes the paper while proposing future research.

2 Related Works

Single Image Super-Resolution (SISR) is a classic problem in digital image processing. Its goal is to increase the resolution of a low-resolution image to obtain a higher-resolution image by restoring high-frequency information. Initially, most SISR reconstructions are based on sample learning; for example, one of the typical methods is the sparse coding method [7]. This approach generally extracts image features first and encodes them into a low-resolution dictionary. The sparse coefficients are passed to the high-resolution dictionary to reconstruct the high-resolution parts, which are then aggregated as a result. These SR methods focus on dictionary learning and optimization or model building and are rarely optimized or considered as a unified optimization framework focusing on the utility of Generative models.

Convolutional Neural Network (CNN)-based methods have greatly improved the performance of SISR [39]. Numerous studies have emerged to converge faster and perform better. Dong et al. pioneered the use of CNNs to solve the SISR problem in [39]. They showed that conventional sparse coding-based SR methods existing at the time can be reformulated into a deep CNN, achieving superior performance. This model is divided into three phases, each performed by a convolution: feature mapping, nonlinear feature mapping, and reconstruction to a high-resolution representation. Below a brief description of the most relevant SR techniques used recently which involve CNN.

Dong et al. introduced the SRCNN, a deep learning technique that can reformulate the conventional sparse coding-based SR methods and achieve superior performance [7]. This success led to the development of numerous methods using deep learning in the SR problem. Residual models such as Very Deep Convolutional

Networks (VDCN) [16], Deeply-Recursive Convolutional Networks (DRCN) [17], and Deep Recursive Residual Network (DRRN) [30] emerged, building the neural network based on units or blocks that learn through residual functions, which represent the difference between the original and processed image. Residual networks can converge faster, requiring fewer epochs and providing a higher Peak Signal-to-Noise Ratio (PSNR) [15] in training, which quantitatively measures the quality of the image reconstruction.

Subsequently, several models have emerged that implement novel scaling techniques for low-resolution to high-resolution image reconstruction, enabling the use of low-resolution images as direct input. Some approaches employ a de-convolution layer at the end of the network that directly maps the original low-resolution image to the high-resolution image [8]. Some others approaches extract features from the low-resolution space and maps them to the high-resolution space [28]. These scaling techniques have been leveraged by several residual models, which use residual scaling methods to improve the stability and performance of deep networks. For instance, some models introduce dense hop connections into a very deep network to enable the efficient combination of low-level and high-level features [32]. Alternatively, some models utilize a Residual Dense Block (RDB) as the central component in network construction, where each RDB consists of densely connected layers and local feature fusion with local residual learning [37].

Recent advancements in the field of SR have led to the introduction of Generative Adversarial Networks (GAN) [12]. GANs consist of a generator that produces SR images and a discriminator that evaluates whether the generated image is real or artificial. A good approximation of the high-resolution image is assumed if the discriminator cannot distinguish between the generated image and the original image [29]. Researchers have also developed a new generator that uses long-range connections to efficiently transfer information between remote layers [25]. In addition, a new function in GAN is used as a discriminator to enable the generator to retrieve more detailed textures by learning to infer which image is more realistic [34]. Furthermore, a residual-in-residual (RIR) structure has been proposed to address the low-frequency information removed through multiple hopping connections. This structure incorporates a Channel Attention (CA) mechanism that adaptively rescales channel characteristics by considering channel inter-dependencies [36].

In this paper we have divided in several groups of SR-algorithms based on their network architectures and characteristics within the context of super-resolution techniques. The algorithms are categorized into four sets, each focusing on specific aspects of network design and methodology.

2.1 Residual-based models

Image SR using Very Deep Super-Resolution (VDSR) [16] convolutional networks demonstrate that by cascading small filters many times into a deep network structure, contextual information about large image regions is efficiently exploited. They use residual learning and extremely high learning rates to quickly optimize a very deep

network. Convergence speed is maximized and they use gradient clipping to ensure training stability.

The DRCN [17] is a network with a deep recursive layer (up to 16 recursions) achieving improved performance without introducing new parameters for additional convolutions. Because learning is very difficult with a standard gradient descent method, they proposed two extensions to alleviate the difficulty of training: recursive supervision and skipping connections (shortcuts).

Subsequently, the Deep Recursive Residual Network (DRRN) [30] proposes a deep model (up to 52 convolutional layers) that adopts residual learning to reduce the difficulty of training in a deep networks, improving the performance of the SISR models defined so far, while using fewer parameters.

2.2 Scaling methods

Dong et al. improved the performance of their SRCNN model with single image of giving it practical use in applications demanding real time (24 fps), achieving improved quality and 40 times faster speed. The proposed model, called Fast Super-Resolution Convolutional Neural Network (FSRCNN) [8], improved three aspects: first, it uses a de-convolution layer at the end of the network that directly maps the original low-resolution image to the high-resolution one; second, they reduced the dimension of the input function by reformulating the mapping layer; and third, they adopted smaller filters but more mapping layers.

The Efficient Sub-Pixel Convolutional Neural Network (ESPCN) [28] extracts the feature map in low-resolution space, without having to scale the low-resolution input to high-resolution space, while reducing the computational complexity of the overall SR operation. In addition, they introduced a sub-pixel convolutional layer, capable of learning a vector of filters to scale the final low-resolution feature map to the high-resolution output.

2.3 Residual models integrating new scaling methods

Residual models integrating new scaling methods represent a combination of both the residual model-based approach and the scaling model-based approach. It's a way of incorporating the benefits of both techniques to improve the quality and performance of super resolution algorithms for images. The residual model contributes its ability to learn fine details and features, while the new scaling methods contribute techniques for enhancing image resolution and generating high-quality results. In this sense the following methods described bellow integrate both approaches mentions before, the residual model-based and scaling model-based.

The Enhanced Deep Super-Resolution (EDSR) [20] residual network model was designed with an improvement of the SRResNet model, achieving better results by eliminating unnecessary modules while obtaining a more compact model. They used residual scaling techniques to give stability to the deep model. This method

showed superior performance over state-of-the-art methods on benchmark datasets, becoming the winner of the NTIRE2017 SR Challenge [31].

Another network for SISR image reconstruction is the Laplacian Pyramid Super-Resolution Network (LapSRN) [19]. This model performs a progressive reconstruction of sub-band residuals from high-resolution images. At each level of the pyramid, the model takes coarse resolution feature maps as input, predicts the high-frequency residuals, and uses transposed convolutions to sample at the finer level. By not requiring bicubic interpolation as a preprocessing step, it drastically reduces computational complexity. On the other hand, network training is performed with deep supervision using a robust loss function, achieving high quality reconstruction.

Tong et al. [32] present a novel model for single image SR called SRDenseNet, which introduces dense hopping connections in a deep network. Feature maps from each layer are propagated to all subsequent layers, providing an efficient way to combine low-level and high-level features in order to improve reconstruction performance. Dense hop connections allow short paths from the output directly to each layer, alleviating the vanishing gradient problem of very deep networks. They also integrate de-convolution layers into the network to learn up-sampling filters and speed up the reconstruction process.

The Residual Dense Network (RDN) [37] was proposed to solve one of the problems of deep CNN-based SR models, which is not fully exploiting the use of hierarchical features of low resolution images, having a relatively low performance. RDN defines a very deep network for SR images, with a Residual Dense Block (RDB) as the core element. Each RDB consists of densely connected layers and Local Feature Fusion (LFF) with Local Residual Learning (LRL). The states of all RDBs are concatenated, allowing LFF to obtain local dense features and adaptively retain information. In addition, LFF achieves very high growth rates, stabilizing the formation of larger networks.

Finally, the deep Residual Channel Attention Network (RCAN) [36] has a Residual In Residual (RIR) structure that causes numerous low-frequency information to be removed through multiple hopping connections, allowing the underlying network to concentrate on learning high-frequency information. In addition, it defines a Channel Attention (CA) mechanism to adaptively rescale channel characteristics by considering channel interdependencies.

2.4 Generative adversarial networks

SR Using a Generative Adversarial Network (SRGAN) [29] is the first model that proposes a Generative Adversarial Network (GAN) [12] for SISR. This framework is capable of inferring natural photographic images for ×4 magnification factors. In a GAN model there is a generator that creates SR images and a discriminator that must distinguish whether the high-resolution image is true or artificial. If the discriminator sees no difference between the estimated high-resolution image and the true high-resolution image, the estimate is assumed to be a good approximation of the high-resolution image. The authors create as a generator the SRResNet model,

a residual network of 5 blocks each composed of two conventional blocks (Conv-BN-ReLU).

Another GAN model is the SR with Feature Discrimination (SRFeat) model [25]. It develops a new generator that uses long-range hop connections so that information between remote layers can be transferred more efficiently. Moreover, it uses an image discriminator and a feature discriminator; the latter encourages the generator to produce high-frequency structural features free of noise artifacts.

The Enhanced Super Resolution Generative Adversarial Network (ESRGAN) [34] model improves the visual quality of its predecessor SRGAN model. They present a generator with a multi-block RRDB (Residual in Residual Dense Block) architecture, without Batch Normalization (BN) layers. They use a relativistic GAN as a discriminator, capable of learning to infer whether one image is more realistic than another, instructing the generator to retrieve more detailed textures.

2.5 Comparison of Super-Resolution Models selected from literature

This section provides a concise overview of several SR techniques based on deep learning and generative models. The models were adapted to use CTA, implemented, evaluated and analyzed, as these models were normally used for biological image processing. In previous subsection we presented a classification of these models we can resume in Table 1. Each model evaluated were categorized based on their architectural characteristics and methodology, as it provides a structured approach for understanding their capabilities. The specific strengths and characteristics of these methods align with the challenges of enhancing vascular structure visualization in CTA images.

Table 1 Comparison of SR Models evaluated for CTA images, based on their network architectures and characteristics.

Model	Convolutional model-based	Residual model-based	GAN model-based
SRCNN915	X		
SRCNN955	X		
EDSR	X	X	
RCAN	X	X	
SRGAN	X		X
ESRGAN	X		X

3 Materials and Methods

3.1 Dataset

Supervised learning has a distinguishing feature: it relies on annotated training data, which refers to data that a human subject matter expert has analyzed and labeled [6]. The supervised learning algorithms implemented for this research

generalized patterns to classify unlabeled data. The data used in this study were anonymized CTA medical images of lower extremities in DICOM (Digital Imaging and Communications in Medicine) standart [3]. Computed Tomography (CT) is a medical imaging technique that produces anatomical slices or sections for diagnostic purposes using X-ray radiation [5]. A CT image is comprised of a series of cells known as voxels. Each voxel is assigned a value corresponding to a density or brightness level, reflecting the material or tissue attenuation in the represented spatial area on the Hounsfield scale [2]. CTA serves multiple purposes, including detecting arterial aneurysms, blockages, blood clots, and PAOD [10].

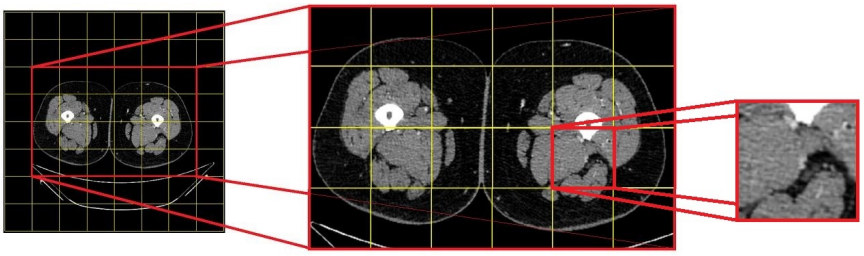

Fig. 2 Cell selection for training and validation. If 600 slices (on average) are selected in a study and from each slice 24 block cells are used, we have about 14,400 64x64 pixel images for training/validation the SR models.

The images obtained by CTA in this study are volumetric data of size 512×512 pixels per slice. Due to the large computational demands of deep learning networks, 64×64 blocks were used for training. The selected block is used as an output image (target), while the input is a bicubic-downsampled version of the same block for testing purpose.

3.2 Image selection

The DICOM model follows a hierarchical structure, where a patient can have one or more studies, each containing several series comprising composite objects like images and presentation states [11]. In this study, we selected the series that included CTA images of the lower extremities from each computed tomography study. We manually removed the initial and final cuts, keeping only the relevant images of interest, which spanned from the genitalia to the ankle. On average, each study/series consisted of about 600 images. Each studey was anonymized. To address memory consumption during the training of SR models, we divided the 512x512 pixel for each slice into smaller 64x64 pixel per block cells. This division strategy prevents memory overflow and ensures smooth execution on workstations. However, since the area under study has specific characteristics, many of these cells do not contain relevant information for the learning process. Therefore, we only selected the cells that contribute the most informative content, as depicted in Figure 2.

3.3 Development Tools

In this study, we used Python as the programming language, along with various packages that facilitate the implementation of artificial intelligence, including Pandas, Numpy, TensorFlow, Keras, sci-kit-learn, and OpenCV-python. We tested the algorithms using Jupyter Notebook. For handling DICOM images, we used the Pydicom library.

The 3D modeling of the original studies and those obtained after applying the SR method was performed with 3D Slicer [9]. This tool is an open-source software designed for the visualization, processing, segmentation, registration, and analysis of 3D medical, biomedical, and other images and meshes.

3.4 Evaluation metrics

Any processing performed on an image can cause a significant loss of information or quality. Several metrics allow to evaluate such loss. PSNR, related to Mean Square Error (MSE), evaluates the quality of the image reconstruction by numerically comparing the original image and the image generated by the reconstruction [27]; it gives a rough estimate of the human perception of the reconstruction quality. Its measure is in decibels (dB), and its value tends to infinity, so the higher it is, the better the quality of the generated image. On the other hand, a lower PSNR value means a big numerical difference between images.

SSIM is a model based on the perception of the human visual system. It measures the similarity between the original and reconstructed image by considering structural information, luminance, and contrast [15]. The SSIM index is a decimal value between -1 and 1, with 0 indicating no structural similarity and 1 indicating a perfectly similar structure, which is achieved in the case of two identical images [23].

3.5 Super-resolution CNN models applied to CTA images

The successful application of deep learning in the SR problem has prompted the development of numerous methods. In this paper, we compared and adapted different SRCNN methods for lower extremity from CTA images. We employ the same loss functions and optimizer as the original authors. We also calculate metrics mentioned in the previous section to quantitatively evaluate the obtained results, including the maximum PSNR [15] and the SSIM [23]. It is worth to mention that in our implemented models, the final convolution, responsible for reconstructing the output image, generates a one-dimensional feature map due to the single-channel (monochrome) images, since for these CTA data are gray-level images. Next, we provide the architecture description for each SR model implemented and evaluated in this work.

Super-resolution convolutional neural network (SRCNN) In 2014, Dong et al. [7] was the first to use the deep learning method to solve SR problems in natural

images. Their method performs direct learning by creating an end-to-end mapping between low-resolution and high-resolution images. They use a CNN that takes the low-resolution image as input and generates the high-resolution image. Fig. 3 shows the architecture of SRCNN 9-1-5 adapted to CTA images. Initially, the low-resolution

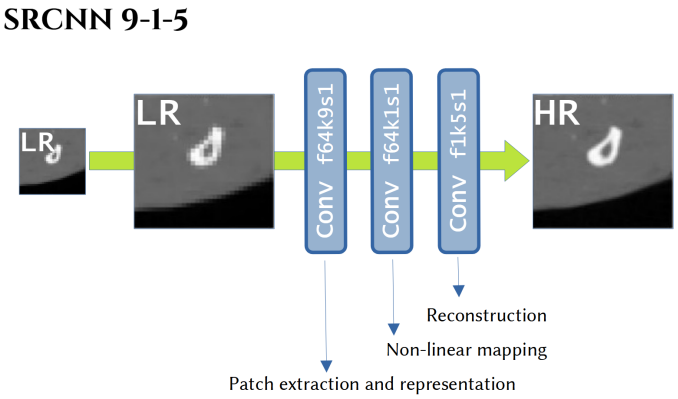

Fig. 3 Implementation scheme of the SRCNN 9-1-5 model. Each convolution is defined by the number of features, the size of the convolution matrix (kernel), and the convolution step (stride).

image is pre-processed by enlarging it to the size of the high-resolution image resulting from bi-cubic interpolation. The end-to-end mapping learning consists of three operations, each performed by a convolution. The first extracts patches from the low-resolution image, each represented as a high-dimensional vector representing image features. It then performs a nonlinear mapping of the vectors to other high-dimensional vectors, defining another set of feature maps. And finally, it reconstructs the high-resolution image by aggregating the previous high-resolution patch representations. In 2015, Dong. et. al published version 3 of the paper [7], where they generalize the second step of their method by applying larger filters, thereby achieving better learning results. Fig. 4 shows the architecture of the SRCNN 9-5-5 model.

Enhanced Deep Residual Networks for Single Image Super-resolution (EDSR) Based on the SRResNet [29], it comprises a sequence of blocks (ResBlock) that consist of a few layers and end with an image scaling block, as depicted in Fig. 5. In contrast to SRResNet, the authors remove the Batch Normalization (BN) layers, significantly enhancing performance without compromising result quality. As a result, they are able to construct deeper networks with superior performance compared to conventional Residual Networks (ResNet) [14]. However, the network training became numerically unstable as the number of feature maps increased beyond a certain threshold. This issue was solved by applying a residual scale with a factor of 0.1 in each block (represented by the 'Mult 0.1' layer in Fig. 5). The final block (Upsample ×2) carries out a ×2 scaling to obtain the high-resolution image. A sequence of 2 such blocks would be used in the ×4 architecture.

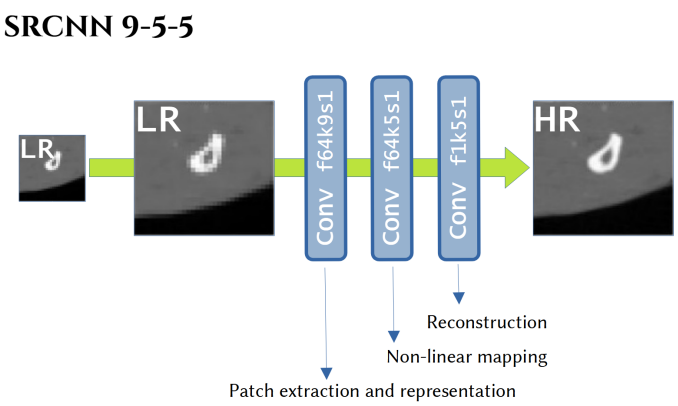

Fig. 4 SRCNN 9-5-5 model architecture.

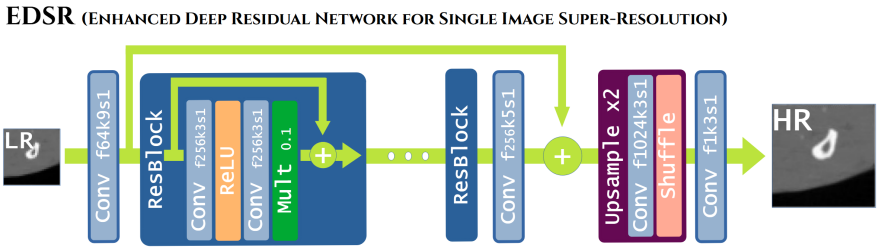

Fig. 5 EDSR model architecture

Residual Channel Attention Networks (RCAN) The Residual Channel Attention Networks (RCAN) model [36] consists of four main parts: shallow feature extraction, residual deep feature extraction (using RIR), scaling module, and reconstruction module. The shallow feature extraction module employs a single convolutional layer. The deep feature extraction involves the development of a new module referred to as the Residual-in-Residual (RIR). This RIR module, which consists of multiple residual groups (RGs), uses a deep residual structure to facilitate the extraction of deep features. The scaling module is carried out using the module proposed in ESPCNN [28], which has proved to be one of the most widely used and a convolution layer for the final reconstruction. This structure allows the training of very deep convolutional neural networks (with more than 400 layers).

The RIR module contains Residual Groups (RG) and a long jump connection. Each RG contains several Residual Channel Attention Blocks (RCAB) and a short hop connection. Residual groups and long-hop connections allow the bulk of the network to focus on more informative components of the low-resolution features. The Channel Attention (CA) mechanism makes the network focus on more informative features by exploiting the inter-dependencies between feature channels.

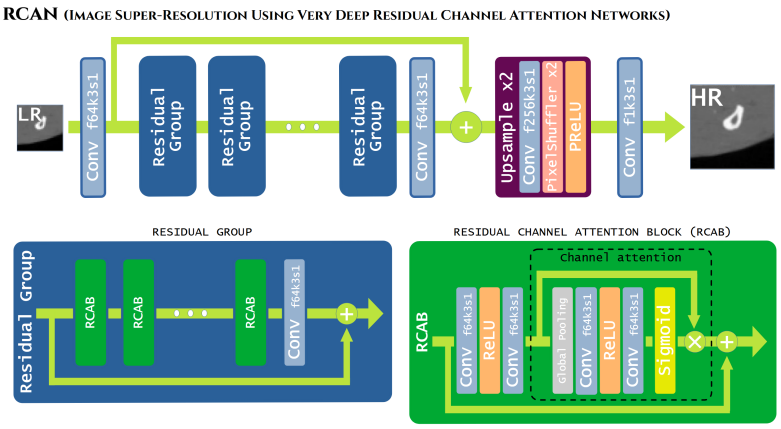

Fig. 6 RCAN model architecture

Super-resolution using generative adversarial networks (SRGAN) In GAN architectures, the value of PSNR decreases, but the overall perceptual quality improves. The objective of this work is to acquire SR images with superior structural quality and generate a dependable 3D reconstruction. Therefore, the researchers in this work refrain from conducting adversarial training on the GAN models and instead focus exclusively on training the generator proposed by the model.

The SRGAN [29] (Super-Resolution Generative Adversarial Networks) model generator, known as SRResNet, is a deep residual network with a hop connection and diverges from MSE as the only optimization objective. The generator architecture, shown in Fig. 7, consists of 16 residual blocks formed by two convolutional layers with small 3×3 convolution matrices and 64-feature maps followed by two batch normalization layers and ParametricReLU (PReLU, Parametric Rectified Linear Unit) as the activation function between these pairs of layers. The final sum of the output and input determines the residual function of the block. The increase in resolution occurs through the concatenation of ×2 scaling blocks based on the desired final result. Shi et al. [28] proposed this scaling block which comprises a 3×3 convolution with 256-feature maps, followed by a pixel blender and PreLU activation function. The final image is obtained by applying a 3×3 convolution and a single feature map corresponding to the channel present in the images processed. The 'tanh' activation function yielded the best results in the conducted tests.

Enhanced Super-Resolution Generative Adversarial Networks (ESRGAN): The enhanced Super-Resolution Generative Adversarial Networks (ESRGAN) [34] arises as an improvement of the image quality generated by SRGAN, mainly by making two modifications to the generator structure: removing all BN layers and designing a new basic block, called Residual in Residual Dense Block (RRDB), which combines a multilevel residual network with dense connections, as shown in Fig. 8.

Removing BN layers has demonstrated improved performance and network generalizability while also reducing computational complexity and memory usage.

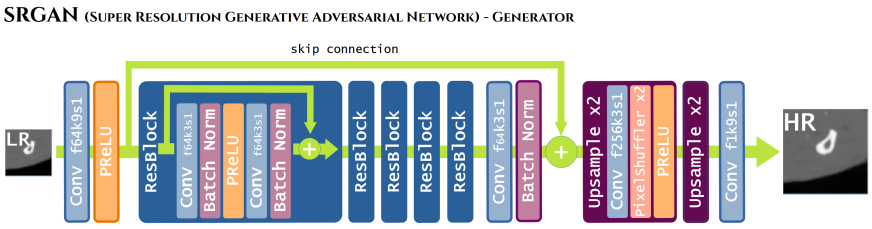

Fig. 7 SRGAN model architecture

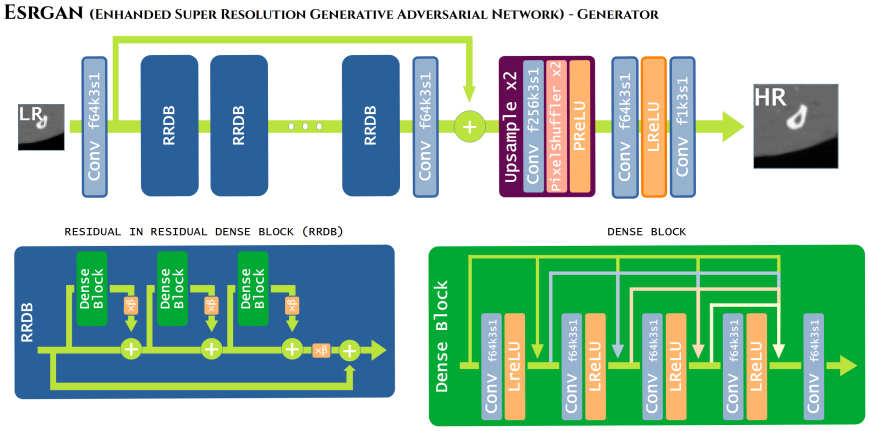

Fig. 8 ESRGAN model architecture.

Furthermore, deep networks exhibit an empirical observation indicating a decreased likelihood of introducing artifacts.

The new basic block proposed in this RRDB model has a deeper and more complex structure than the original SRGAN residual block. It has a residual-in-residual structure where residual learning is performed at different levels using a dense block on the main path, allowing the network capacity to benefit more from the dense connections. Another novelty is the residual scaling, multiplying by a constant β between 0 and 1 before adding them to the main path, thus preventing instability.

4 Results

The training phase of a neural network is crucial in achieving successful outcomes in deep learning, alongside factors such as the quantity and quality of the data. This phase plays a pivotal role in ensuring the appropriateness and efficacy of the produced results.

In order to perform comparative training between the different models selected in this work, the same set of images was used for all of them. Two CTA studies were used, the first study with 596 slices, and 580 slices the second one. The image selection was performed as specified in section 3.2. Twenty percent (20%) of the slices were used for validation, the rest for training. Each slice provides a batch of 8 images of 64×64 pixels. Finally, using 7,528 images for training and 1,880 images for validation. All models were subjected to a 10-epoch training using the parameters defined by their authors in the published papers.

In the GAN networks only the generator network is trained, since a GAN training with discriminator brings visual realism to the images but introduces artifacts in the image [29, 34], especially in tiny structures, which could affect its use for medical diagnosis [35]. An ×8-scale training was performed for the models (SRCNN 9-5-5) that computationally allowed it for the resources we had available, but the quantitative and qualitative results were so poor that they did not deserve to be shown. The results of the training performed at ×2 and ×4 scale for all selected models are shown below.

The bicubic interpolation is not a neural network model but a mathematical model used to perform image scaling, and we used it as a reference. For an unknown point in the enlarged image, its calculated value is a function of the value of the 16 points of the original image surrounding it and the distance separating it [13]. The diagram of the bicubic interpolation algorithm is shown in Fig. 9. Still, it has been implemented as another model thanks to the Keras Lambda function to homogenize the study and obtain the comparison metrics. Table 2 displays the PSNR and SSIM values for

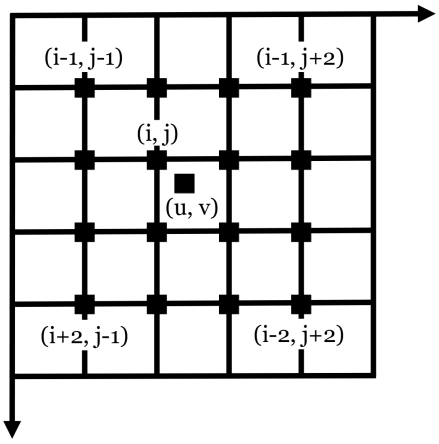

Fig. 9 Diagram of bicubic interpolation algorithm [13].

scales x2 and x4, from every method studied. The observed trend reveals a decrease in visual quality starting from the ×4 scale, every model showed better results on scale x2.

The SRCNN model, characterized by its simplicity with just three convolutions, demonstrates notable performance compared to the other implemented models for

this image type. The SRCNN 9-5-5 model, which consists of a 5×5 convolution matrix in the central convolution, performs lighter better than its sister model (see Table 2). However, it is not possible to say which of them perform better.

Although the EDSR model was developed as an enhancement of the SRRestNet model (SRGAN generator), it has exhibited inferior results, particularly at the ×4 scale, where the difference is significantly noticeable both in qualitative and quantitative terms. Please refer to Table 2 for a detailed presentation of the results.

The authors of RCAN defined in their paper a model configuration of 10 RG with 20 RCAB each. However, after testing several configurations in this study, better results have been obtained with 2 RGs and 20 RCABs each. These results are shown in Table 2.

The SRGAN model defines a generator (SRResNet) that has been taken as a reference in the literature due to its quality, especially at scales ×4 or larger. This model with momentum equal to 0.5 in the BatchNormalization, as used by the creators, the PSNR and SSIM were very good, but generated large artifacts in most of the images for x4 scale and degenerated their 3D representation. But we realized after several testing than reducing the momentum to 0.2, which, in our case, it does not generate artifacts at x4 scale and obtains better results, although not as good, than the RCAN model. The results obtained in the training of this model reflected in Table 2 showed that on CTA images with the scale x4 it performs better than the scale x2 compared with RCAN model, as we can see in Table 2, but there was not so much difference. However SRGAN is slightly better in the scale x4 than RCAN. As conclusion SRGAN perfomed better than the others models compared including the RCAN in scale x4 (see Table 2).

The ESRGAN model is considered by the literature as an improvement of its predecessor SRGAN, using a full GAN (generator-discriminator) training. In this study only the generator of the models is used for reasons already defined, with 64 features and 23 RRDB blocks. In this case we have worse results than its predecessor, as can be seen in Table 2.

5 Discussion

The compared models allow obtaining better results at PSNR and SSIM level than the mathematical scaling models such as the bicubic one. We can observe in Table 2 that, for this type of images with a single channel, at ×2 scale even better results are obtained than with color images, if we consider the results obtained by the authors of the models reflected in the literature [7, 20, 29, 34, 36]. Table 2 shows the results for scale ×2, and x4. The better result for scale x2 was shown by RCAN model, and for scale x4 the better results is gotten for the SRGAN model. Using the RCAN and SRGAN models, the best SR models compared for ×2 and ×4 scales, respectively, we can test the effect of SR on computed tomography angiographic (CTA) images of the lower extremities. If we perform a 3D representation of the images obtained we can see how the small arteries gain light due to the effect of the SR, as we can see in Figures 10, 11, and 12.

Table 2 Summary table of the results obtained by the applied methods with the metrics obtained at scales x2 and x4, tested on three different patients in the same arterial area.

Patient 2		**Patient 3**		**Patient 4**	
Original ROI					
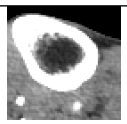		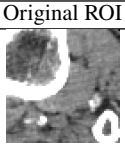		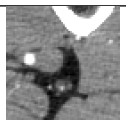	
x2 scale	**x4 scale**	**x2 scale**	**x4 scale**	**x2 scale**	**x4 scale**
BICUBIC					
	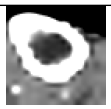				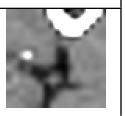
PSNR 35.93 SSIM 0.9796	PSNR 27.03 SSIM 0.8670	PSNR 35.39 SSIM 0.9746	PSNR 26.37 SSIM 0.8518	PSNR 40.16 SSIM 0.9819	PSNR 32.95 SSIM 0.9415
SRCNN 9-1-5					
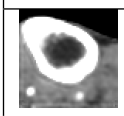	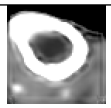	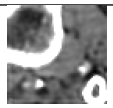			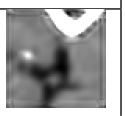
PSNR 36.66 SSIM 0.9814	PSNR 28.48 SSIM 0.9305	PSNR 36.20 SSIM 0.9753	PSNR 27.49 SSIM 0.8735	PSNR 40.91 SSIM 0.9813	PSNR 34.53 SSIM 0.9433
SRCNN 9-5-5					
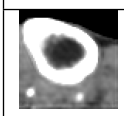	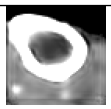	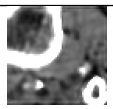			
PSNR 35.71 SSIM 0.9786	PSNR 28.23 SSIM 0.8981	PSNR 35.69 SSIM 0.9746	PSNR 27.84 SSIM 0.8831	PSNR 39.48 SSIM 0.9802	PSNR 33.58 SSIM 0.9422
EDSR					
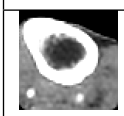	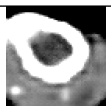		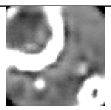		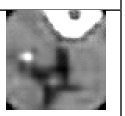
PSNR 37.56 SSIM 0.9868	PSNR 25.70 SSIM 0.8472	PSNR 34.79 SSIM 0.9813	PSNR 24.29 SSIM 0.8362	PSNR 38.22 SSIM 0.9850	PSNR 29.84 SSIM 0.9323
RCAN					
	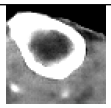		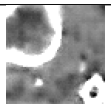		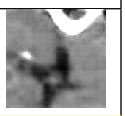
PSNR 41.82 SSIM 0.9903	PSNR 31.55 SSIM 0.9422	PSNR 41.16 SSIM 0.9845	PSNR 29.09 SSIM 0.9107	PSNR 46.21 SSIM 0.9865	PSNR 36.32 SSIM 0.9527
SRGAN					
	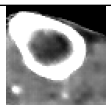				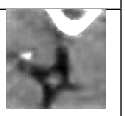
PSNR 40.85 SSIM 0.9897	PSNR 31.97 SSIM 0.9500	PSNR 40.50 SSIM 0.9846	PSNR 30.18 SSIM 0.9196	PSNR 44.60 SSIM 0.9860	PSNR 36.36 SSIM 0.9537
ESRGAN					
					
PSNR 35.65 SSIM 0.9789	PSNR 25.45 SSIM 0.8172	PSNR 33.03 SSIM 0.9730	PSNR 25.06 SSIM 0.8166	PSNR 36.65 SSIM 0.9804	PSNR 28.26 SSIM 0.9166

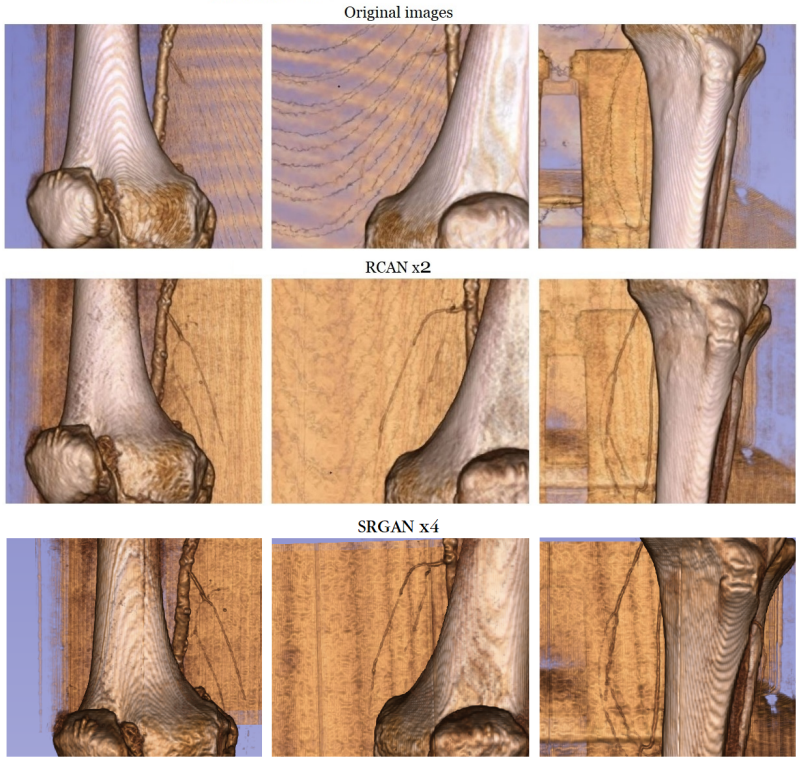

Fig. 10 3D visualization of the effect of SR (Patient 5). The first row of images the original images, second row the best result with RCAN model at scale x2, and the third row the best result with SRGAN model at scale x4.

6 Conclusion and Future Work

In this study, we addressed the limitations of standard CTA in capturing the detailed morphology of small arteries, particularly in the lower extremities. To overcome this challenge, we applied advanced super-resolution (SR) techniques to enhance the three-dimensional (3D) reconstruction and visualization of lower extremity arteries using standard CTA images. We evaluated various single-image super-resolution (SISR) models tailored for CTA images, including SRCNN, EDSR, RCAN, SRGAN, and ESRGAN. Among them, the RCAN (Residual Channel Attention Networks) and SRGAN (Super-Resolution Generative Adversarial Network) models stood out as the most effective. RCAN excelled at a two-times (x2) scale, while SRGAN performed exceptionally well at a four-times (x4) scale. These models have different objectives, with RCAN focusing on improving high-resolution image quality and SRGAN specialized in upscaling low-resolution images.

Our findings demonstrate that these SR techniques significantly improved image quality and enabled the visualization of previously indistinct or imperceptible arteries, which holds promise for conditions like peripheral arterial occlusive disease

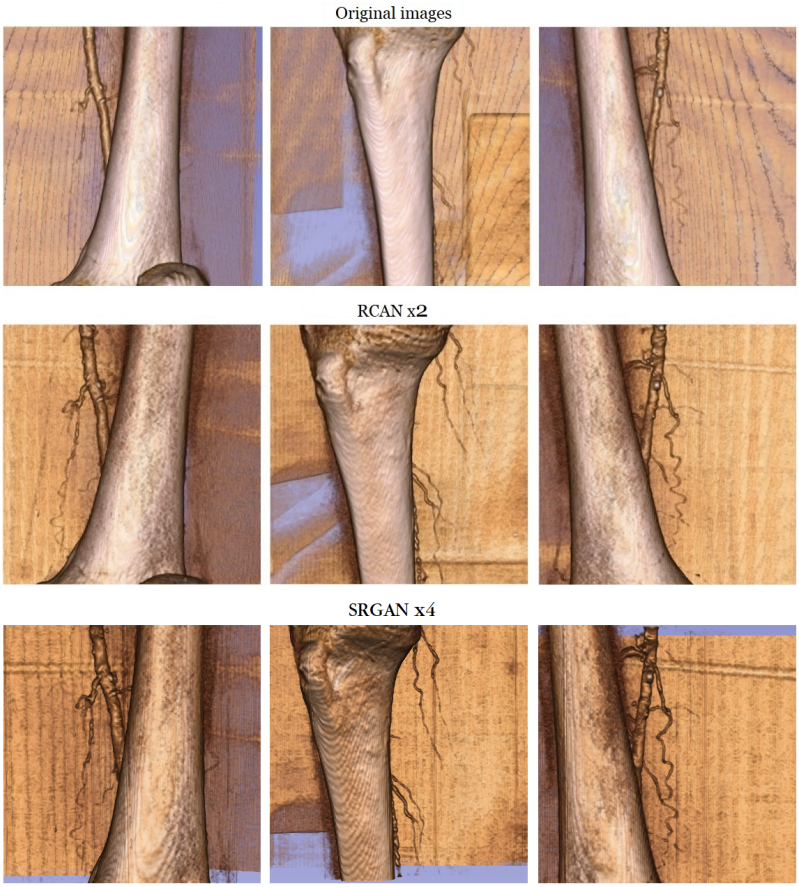

Fig. 11 3D visualization of the SR effect (Patient 6), also with best results with RCAN and SRGAN models (x2 ans x4 scale respectively).

(PAOD). This advancement underscores the role of intelligent systems in enhancing medical diagnostics and decision support. This chapter exemplifies how cutting-edge technologies in artificial intelligence and machine learning can transform healthcare by providing clinicians with powerful tools to analyze complex information and make more informed decisions, showcasing intelligent systems that support decision-making across various fields.

Future research should explore the application of SR methods to enhance inter-slice quality in CTA images, as this could provide additional diagnostic insights into arterial diseases. Despite challenges such as computational cost and time constraints, our study highlights the potential of SR techniques as a valuable tool for diagnosing PAOD. By integrating these advanced techniques into clinical practice, we can improve diagnostic capabilities in vascular imaging, ultimately leading to better decision-making and patient outcomes.

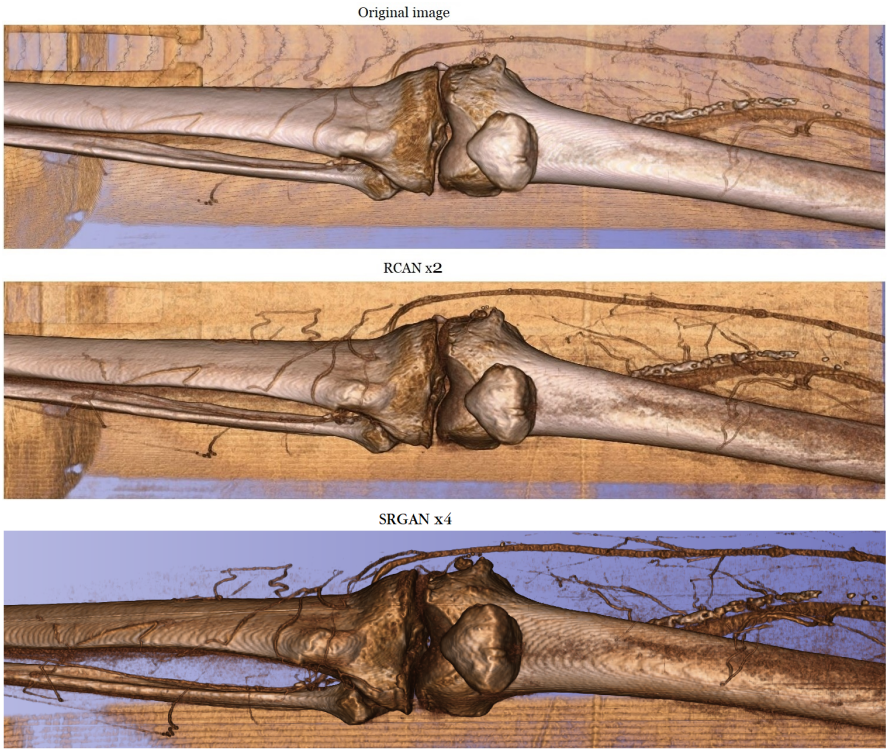

Fig. 12 3D visualization of the SR effect (Patient 7), also with best results with RCAN and SRGAN models (x2 ans x4 scale respectively).

Acknowledgements The authors would like to express their sincere gratitude to Universidad de Ibagué for their invaluable collaboration ad honorem of this research. Additionally, we extend our appreciation to Universidad Internacional de Valencia in Spain, Universidad Simón Bolívar in Caracas, Venezuela, and Tecnológico de Monterrey in Mexico for their support and contributions.

Competing Interests The authors have no conflicts of interest to declare that are relevant to the content of this chapter.

Ethics Approval In compliance with ethical standards and regulations, this study exclusively utilized anonymized patient data obtained from Medical University of Vienna during a reserach work between 2002 and 2006. Prior to data collection, all identifiable information was removed to protect patient confidentiality and privacy. The anonymization process ensured that individual identities could not be discerned from the dataset used in this research. Additionally, this study adheres to the principles outlined in the Declaration of Helsinki. Noting that the use of anonymized patient data without explicit consent is widely accepted in research practices, particularly when adherence to strict anonymization protocols and ethical standards is maintained. By prioritizing patient privacy and confidentiality, while upholding the integrity of scientific inquiry, this study endeavors to generate valuable insights for the benefit of both current and future patients.

References

1. Bolaños Martínez, I., Chaves Chaves, A., Gallón Vanegas, L., Ibañez Morera, M., López Barquero, H.: Enfermedad arterial periférica en miembros inferiores. Medicina Legal de Costa Rica **36**(1), 84–90 (2019)
2. Calzado, A., Geleijns, J.: Tomografía computarizada. evolución, principios técnicos y aplicaciones. Revista de Física Médica **11**(3) (2010)
3. Chin, H., Klepac, D., Ernst, R.D., et al.: Digital photography of digital imaging and communications in medicine—3 images from computers in the radiologist's office. J Digit Imaging (1999)
4. Clement, D.: Medical treatment of peripheral artery occlusive disease (paod). Acta Chirurgica Belgica **100**(5), 190–193 (2000)
5. Costa, J., Soria, J.: Tomografía Computarizada dirigida a Técnicos Superiores en Imagen para el Diagnóstico. Fotoletra, S.A. (2015)
6. Cunningham, P., Cord, M., Delany, S.J.: Supervised Learning, pp. 21–49. Springer Berlin Heidelberg, Berlin, Heidelberg (2008). DOI 10.1007/978-3-540-75171-7_2
7. Dong, C., Loy, C.C., He, K., Tang, X.: Learning a deep convolutional network for image super-resolution. In: D. Fleet, T. Pajdla, B. Schiele, T. Tuytelaars (eds.) Computer Vision – ECCV 2014, pp. 184–199. Springer International Publishing, Cham (2014)
8. Dong, C., Loy, C.C., Tang, X.: Accelerating the super-resolution convolutional neural network (2016)
9. Fedorov, A., Beichel, R., Kalpathy-Cramer, J., Finet, J., Fillion-Robin, J.C., Pujol, S., Bauer, C., Jennings, D., Fennessy, F.M., Sonka, M., Buatti, J., Aylward, S.R., Miller, J.V., Pieper, S., Kikinis, R.: 3d slicer as an image computing platform for the quantitative imaging network. Magnetic Resonance Imaging **30**(9), 1323–1341 (2012)
10. Fleischmann, D., Lammer, J.: Peripheral ct angiography for interventional treatment planning. Eur Radiol Suppl **16**, M58–M64 (2006). DOI 10.1007/s10406-006-0197-y
11. Gibaud, B.: The dicom standard: A brief overview. In: Y. Lemoigne, A. Caner (eds.) Molecular Imaging: Computer Reconstruction and Practice, pp. 229–238. Springer Netherlands, Dordrecht (2008)
12. Goodfellow, I.J., Pouget-Abadie, J., Mirza, M., Xu, B., Warde-Farley, D., Ozair, S., Courville, A., Bengio, Y.: Generative adversarial networks (2014)
13. Han, D.: Comparison of commonly used image interpolation methods. In: Proceedings of the 2nd International Conference on Computer Science and Electronics Engineering (ICCSEE 2013), pp. 1556–1559. Atlantis Press (2013). DOI 10.2991/iccsee.2013.391
14. He, K., Zhang, X., Ren, S., Sun, J.: Deep residual learning for image recognition. In: 2016 IEEE Conference on Computer Vision and Pattern Recognition (CVPR), pp. 770–778 (2016). DOI 10.1109/CVPR.2016.90
15. Horé, A., Ziou, D.: Image quality metrics: Psnr vs. ssim. In: 2010 20th International Conference on Pattern Recognition, pp. 2366–2369 (2010). DOI 10.1109/ICPR.2010.579
16. Kim, J., Lee, J., Lee, K.: Accurate image super-resolution using very deep convolutional networks. In: 2016 IEEE Conference on Computer Vision and Pattern Recognition (CVPR), pp. 1646–1654. IEEE Computer Society, Los Alamitos, CA, USA (2016). DOI 10.1109/CVPR.2016.182. URL https://doi.ieeecomputersociety.org/10.1109/CVPR.2016.182
17. Kim, J., Lee, J.K., Lee, K.M.: Deeply-recursive convolutional network for image super-resolution. In: 2016 IEEE Conference on Computer Vision and Pattern Recognition (CVPR), pp. 1637–1645 (2016). DOI 10.1109/CVPR.2016.181
18. La Cruz, A., Straka, M., Kochl, A., Sramek, M., Groller, E., Fleischmann, D.: Non-linear model fitting to parameterize diseased blood vessels. In: IEEE Visualization 2004, pp. 393–400 (2004). DOI 10.1109/VISUAL.2004.72
19. Lai, W.S., Huang, J.B., Ahuja, N., Yang, M.H.: Deep laplacian pyramid networks for fast and accurate super-resolution (2017)
20. Lim, B., Son, S., Kim, H., Nah, S., Lee, K.M.: Enhanced deep residual networks for single image super-resolution (2017)

21. Nakanishi, R., Motoyama, S., Leipsic, J., Budoff, M.J.: How accurate is atherosclerosis imaging by coronary computed tomography angiography? Journal of Cardiovascular Computed Tomography **13**, 254–260 (2019). DOI 10.1016/j.jcct.2019.06.005
22. Napoli, A., Fleischmann, D., Chan, F.P., Catalano, C., C., H.J., Passariello, R., Rubin, G.D.: Computed tomography angiography. Journal of Computer Assisted Tomography **28**, S32–S45 (2004). DOI 10.1097/01.rct.0000120859.80935.10
23. Ndajah, P., Kikuchi, H., Yukawa, M., Watanabe, H., Muramatsu, S.: Ssim image quality metric for denoised images. In: Proceedings of the 3rd WSEAS International Conference on Visualization, Imaging and Simulation, VIS '10, p. 53–57. World Scientific and Engineering Academy and Society (WSEAS), Stevens Point, Wisconsin, USA (2010)
24. Norgren, L., Hiatt, W., Dormandy, J., Nehler, M., Harris, K., Fowkes, F.: Inter-society consensus for the management of peripheral arterial disease (tasc ii). European Journal of Vascular and Endovascular Surgery **33**(1), S1–S75 (2007). DOI 10.1016/j.ejvs.2006.09.024. Supplement
25. Park, S.J., Son, H., Cho, S., Hong, K.S., Lee, S.: Srfeat: Single image super-resolution with feature discrimination. In: V. Ferrari, M. Hebert, C. Sminchisescu, Y. Weiss (eds.) Computer Vision – ECCV 2018, pp. 455–471. Springer International Publishing, Cham (2018)
26. Preim, B., Oeltze, S.: 3d visualization of vasculature: An overview. In: L. Linsen, H. Hagen, B. Hamann (eds.) Visualization in Medicine and Life Sciences, pp. 39–59. Springer Berlin Heidelberg, Berlin, Heidelberg (2008)
27. Sara, U., Akter, M., Uddin, M.: Image quality assessment through fsim, ssim, mse and psnr—a comparative study. Journal of Computer and Communications **7**, 8–18 (2019). DOI 10.4236/jcc.2019.73002
28. Shi, W., Caballero, J., Huszar, F., Totz, J., Aitken, A.P., Bishop, R., Rueckert, D., Wang, Z.: Real-time single image and video super-resolution using an efficient sub-pixel convolutional neural network. In: 2016 IEEE Conference on Computer Vision and Pattern Recognition (CVPR), pp. 1874–1883. IEEE Computer Society, Los Alamitos, CA, USA (2016). DOI 10.1109/CVPR.2016.207. URL https://doi.ieeecomputersociety.org/10.1109/CVPR.2016.207
29. Shi, W., Caballero, J., Huszár, F., Totz, J., Aitken, A.P., Bishop, R., Rueckert, D., Wang, Z.: Real-time single image and video super-resolution using an efficient sub-pixel convolutional neural network (2016)
30. Tai, Y., Yang, J., Liu, X.: Image super-resolution via deep recursive residual network. In: 2017 IEEE Conference on Computer Vision and Pattern Recognition (CVPR), pp. 2790–2798 (2017). DOI 10.1109/CVPR.2017.298
31. Timofte, R., Agustsson, E., Gool, L.V., et al.: Ntire 2017 challenge on single image super-resolution: Methods and results. In: 2017 IEEE Conference on Computer Vision and Pattern Recognition Workshops (CVPRW), pp. 1110–1121 (2017). DOI 10.1109/CVPRW.2017.149
32. Tong, T., Li, G., Liu, X., Gao, Q.: Image super-resolution using dense skip connections. In: 2017 IEEE International Conference on Computer Vision (ICCV), pp. 4809–4817 (2017). DOI 10.1109/ICCV.2017.514
33. Uhl, J.F., Prat, G., Costi, D., Ovelar, J.A., Scarpelli, F., Ruiz, C., Lorea, B.: Modelado 3d del sistema vascular. Flebología **44**, 17–27 (2018)
34. Wang, X., Yu, K., Wu, S., Gu, J., Liu, Y., Dong, C., Loy, C.C., Qiao, Y., Tang, X.: Esrgan: Enhanced super-resolution generative adversarial networks (2018)
35. You, C., Cong, W., Vannier, M.W., Saha, P.K., Hoffman, E.A., Wang, G., Li, G., Zhang, Y., Zhang, X., Shan, H., Li, M., Ju, S., Zhao, Z., Zhang, Z.: CT super-resolution GAN constrained by the identical, residual, and cycle learning ensemble (GAN-CIRCLE). IEEE Transactions on Medical Imaging **39**(1), 188–203 (2020). DOI 10.1109/tmi.2019.2922960
36. Zhang, Y., Li, K., Li, K., Wang, L., Zhong, B., Fu, Y.: Image super-resolution using very deep residual channel attention networks. In: V. Ferrari, M. Hebert, C. Sminchisescu, Y. Weiss (eds.) Computer Vision – ECCV 2018, pp. 294–310. Springer International Publishing, Cham (2018)
37. Zhang, Y., Tian, Y., Kong, Y., Zhong, B., Fu, Y.: Residual dense network for image super-resolution (2018)

38. Zhou, L., Fan, M., Hansen, C., Johnson, C.R., Weiskopf, D.: A review of three-dimensional medical image visualization. Health Data Science **2022**, 9840519 (2022). DOI 10.34133/2022/9840519. URL https://spj.science.org/doi/abs/10.34133/2022/9840519
39. Zhu, H., Xie, C., Fei, Y., Tao, H.: Attention mechanisms in cnn-based single image super-resolution: A brief review and a new perspective. Electronics **10**(10) (2021). DOI 10.3390/electronics10101187. URL https://www.mdpi.com/2079-9292/10/10/1187